Methods 256 (2026) 149–159

Contents lists available at ScienceDirect

Methods

journal homepage: www.elsevier.com/locate/ymeth

Experimental platform to study the neuronal mechanisms of magnetoreception in the honey bee☆

Alan Oesterle [a], Alara Kiriş [b,c], Albrecht Haase [a,c,*]

[a] Department of Physics, University of Trento, Trento, Italy
[b] Institute of Physics, École Polytechnique fédérale de Lausanne, Lausanne, Switzerland
[c] Center for Mind/Brain Sciences, University of Trento, Rovereto, Italy

ARTICLE INFO

Keywords:
Magnetoreception
Two-photon calcium imaging
Honeybee
Anterior optic tubercle
Magnetic field stimulation

ABSTRACT

Honey bees (*Apis mellifera*) offer an alternative model for investigating magnetoreception, exhibiting reliable navigation and behavioral responses to magnetic fields. Thanks to their compact brains, well-matched to the penetration depth of modern optical imaging techniques, they may offer insights into the neural and biochemical mechanisms underlying this sense, something that standard models, like migrating birds, have not so far provided. But also in honeybees, this progress requires tools capable of resolving weak, magnetically induced neural activity with high spatio-temporal precision. The approach, presented here, bridges quantum biology and neuroscience, aiming at testing the radical pair mechanism (RPM) as a potential basis for magnetic sensing. As the RPM predicts that magnetoreception is coupled to the visual system, we developed an *in vivo* two-photon calcium imaging approach to measure neural activity in the anterior optic tubercle, a higher-order visual center involved in chromatic processing and potentially navigation. Bees were prepared using a minimally invasive technique, in which this neuropil was retrogradely labelled with a fluorescent calcium indicator, enabling stable recording conditions over several hours. Controlled blue-light stimuli were provided by the scattered output of a fiber laser, and weak magnetic-field stimuli were applied by a shielded, three-axis Helmholtz coil system that allowed precise modulation of field strength and polarity while minimizing electromagnetic interference. Visual stimulation evoked consistent and reproducible calcium responses, validating the preparation and imaging stability. Magnetic stimulation produced small decreases in the calcium-response signal in single individuals without statistical significance, which might be the first indications of field-dependent modulation of neural activity. The developed imaging framework will allow thorough testing of magnetic modulation in vision- and navigation-related brain regions, providing a platform for controlled tests of RPM-specific predictions, including light dependence, polarity independence, and radiofrequency perturbation. By targeting other brain regions, the platform can also be adapted to test alternative mechanisms beyond the visually mediated RPM hypothesis, like putative magnetite-based sensing in the bee's abdomen, as implicated by previous studies.

1. Introduction

To understand how animals detect and process the Earth's magnetic field, one must take on the unique challenge of investigating the molecular and neural processes that link quantum-biological mechanisms to behavioral outputs [1]. Magnetoreception has been demonstrated across a wide range of taxa, including birds [2], rodents [3], sea turtles [4], and several invertebrates, such as fruit flies [5], ants [6], butterflies [7], cockroaches [8], and lobsters [9]. Despite this breadth of evidence, the mechanistic basis of magnetoreception and the associated neural pathways remain incompletely understood [10].

The honeybee (*Apis mellifera*) constitutes a particularly advantageous model organism for investigating these processes. Honeybees forage over distances exceeding 10 km [11] and rely on the integration of multiple navigational cues [12–14]. Behavioral evidence for magnetic field sensitivity has been reported in this species by multiple independent studies [15–21], and their well-characterized neuroanatomy [22] makes them well-suited for studying the neural correlates of magnetic sensing. Despite the substantial behavioral evidence of magnetic field perception in honey bees, the mechanism and anatomical location of

☆ This article is part of a special issue entitled: 'Editors Collection - YMETH' published in Methods.

* Corresponding author at: Center for Mind/Brain Sciences, University of Trento, Rovereto, Italy.
E-mail address: albrecht.haase@unitn.it (A. Haase).

https://doi.org/10.1016/j.ymeth.2026.09.005
Received 5 May 2026; Received in revised form 31 August 2026; Accepted 29 September 2026
Available online 30 September 2026
1046-2023/© 2026 The Authors. Published by Elsevier Inc. This is an open access article under the CC BY license (http://creativecommons.org/licenses/by/4.0/).

potential receptors and the neural processing pathway remain unresolved. While magnetic material has been detected in the abdomen and antennae of bees [23–26], studies in butterflies and cockroaches suggest possible ocular involvement [27,28]. However, these findings cannot be directly generalized to honey bees.

Three principal hypotheses have been proposed to explain magnetoreception [29,30]: magnetite-based mechanisms [31,32], electromagnetic induction [33], the radical pair mechanism (RPM) [34,35], or hybrid systems [36]. Although the RPM currently represents the most extensively investigated and widely supported model, evidence consistent with magnetite-based and induction-based mechanisms continues to emerge [37,38]. The RPM posits that magnetoreception arises from light-dependent photochemical reactions generating long-lived, spin-correlated radical pairs [29]. These radical pairs are sensitive to magnetic fields as weak as the Earth's magnetic field (≈ 0.5 G), resulting in magnetically dependent changes in reaction yields that may influence downstream neural activity. Consistent with the observed light dependence of magnetoreception, it has been proposed that these reactions occur within the blue-light photoreceptor cryptochrome (CRY) [27,35,39–43]. Because cryptochrome is expressed in the retina, magnetic sensing has been hypothesized to interact with visual processing pathways, potentially manifesting as a modulation of visual input, perceived as a light-dark pattern superimposed onto the normal visual field [44,45].

To date, experimental investigations of the RPM have largely focused on behaviour [46,47], *in vitro* experiments [43,48], or heterologous expression of CRY outside its native cellular context [49]. In contrast, there are currently no tools available to directly measure magnetic-field-dependent neural activity in intact central brain circuits under controlled and physiologically relevant conditions. *In vivo* imaging approaches capable of resolving neuronal activity in central brain regions are predestined to address this gap [50–52].

Two-photon calcium imaging provides high spatiotemporal resolution and sufficient imaging depth to access neuronal activity in intact brain tissue [53]. The confined excitation volume reduces photobleaching and phototoxicity, while near-infrared excitation enables imaging at depths approaching 1 mm in scattering tissue [54]. Given that the honeybee brain has a volume of approximately 1 mm^3 [22], this approach enables functional imaging across large portions of the brain, unlike in migrating birds, the standard model in magnetoreception research, whose larger brains limit optical access.

In this study, based on methods developed in previous studies [55–57], we establish an approach for *in vivo* two-photon calcium imaging of neuronal activity in the anterior optic tubercle (AOTu), a higher-order visual processing center involved in chromatic processing and navigation [58–62]. The AOTu receives input from the optic lobes via the anterior optic tract and is interconnected across hemispheres through the ventral intertubercular tract (vITT). Targeting this region may enable the investigation of magnetically mediated signals beyond the retina, providing access to neural circuits where signal integration and amplification occur naturally. This approach may open new avenues for research in magnetoreception, facilitating the exploration of downstream neural processing of weak primary signals, and providing a framework for examining how weak magnetic cues are transduced and integrated in the brain. The present study does not test a specific magnetoreception hypothesis or assign the magnetic sensor to a particular anatomical structure. It rather introduces the methods that can be used to study the involvement of the visual system. The platform, however, is designed so that it allows for future tests also of alternative sensory locations and mechanisms.

2. Methods

2.1. Bee preparation

Worker bees (*Apis mellifera*) were collected at the hive entrance from 3 colonies located at the apiary of the Center for Mind/Brain Sciences in Rovereto.

The honeybee preparation protocol was developed based on previous methods to image the bee's visual system [60] and olfactory system [63].

2.1.1. Neuronal staining protocol

1) Returning foragers were collected at the hive entrance between 10 am and 12 pm using a small plastic container. Bees were fed 5-6 μL of 50% (w/w) sucrose solution to maintain viability during preparation.
2) Bees were immobilized by chilling on ice until they stopped moving and were then mounted in a custom Plexiglass holder (Fig. 1). To stabilize the head, a wedge of soft dental wax (Zeta) was inserted between the head and the mount and shaped accordingly. The thorax was supported with a posterior sponge to limit body movement.
3) Antennae were restrained with thin, bent copper wires and secured at the base with n-eicosane (Thermo Fisher Scientific). The copper wires were then removed.
4) To expose the brain, a rectangular window was cut into a section of the head cuticle with a knife made from double-edged razor blades, which was secured in a razor blade holder (WPI).
5) The left salivary glands were displaced or removed, and tracheal segments adjacent to the left AOTu were carefully displaced to provide access for dye injection (Fig. 2A).
6) Crystallized Fura-dextran (10.000 MW, ThermoFisher Scientific) was loaded onto the tips of three borosilicate glass needles produced with a Pipette puller (Narishige) to a tip size of approximately 5 μm (Fig. 2B) and injected into the left AOTu using the mushroom body α-lobe as a landmark, as it has a slightly darker tone than the surrounding tissue (Fig. 2A).
7) The removed cuticle was replaced, and bees were fed an additional 3 μL of 50% (w/w) sucrose solution. Following injection, bees were maintained overnight in a dark, humid chamber to allow dye diffusion into the contralateral AOTu via the ventral intermediate tract (vITT).

2.1.2. Imaging preparation protocol

1) The following morning, mandibles were immobilized with n-eicosane to minimize movement (Fig. 3). The head capsule was reopened, and the salivary glands and tracheae overlaying the right AOTu were carefully displaced.
2) Surface hemolymph was absorbed with tissue, and the head capsule was sealed with a droplet of transparent two-component silicone (Kwik-Sil, WPI). Before curing, a thin plastic sheet was placed in contact with the silicone, with edges bent upward, and coated with black acrylic paint, leaving a small observation window (Fig. 4A,B).
3) The bee was positioned under the objective of the two-photon microscope (Fig. 4C), with a water droplet placed between the water-immersion lens and the observation window.

This preparation enables stable recordings of neural activity for 3–4 hours, after which responses progressively diminish.

2.2. Visual stimulation setup

The visual stimulus was generated by a modulatable 473 nm diode laser (iBeam smart 473, TOPTICA) coupled to an optical fiber, providing up to 55 mW output power. The beam entered through an opening in the aluminum housing and was scattered by the rear panel, resulting in a diffuse, uniform illumination of the side panel, the visual field of the bee eye, which was enhanced by placing sheet of white paper on the surface (Fig. 5). The photon flux incident on the bee's eye, measured with an amplified photodiode, was approximately 4×10^{17} photons $m^{-2}s^{-1}$,

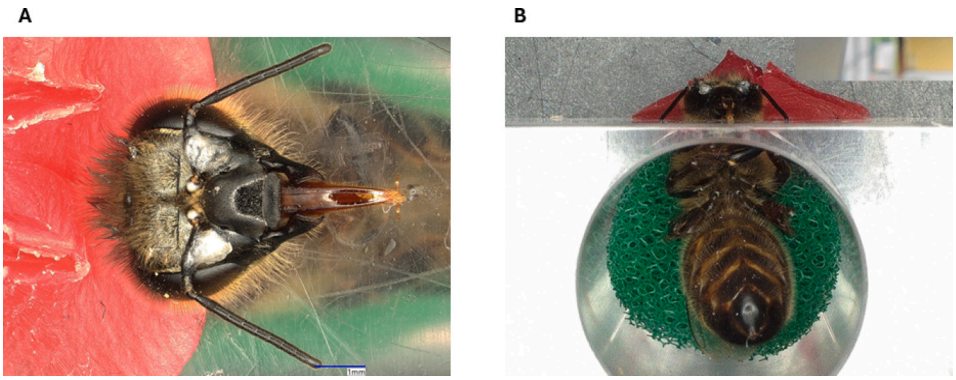


Fig. 1. (A) Head fixation to the plexiglass mount with soft dental wax (red), (B) Thorax supported with a sponge (green).

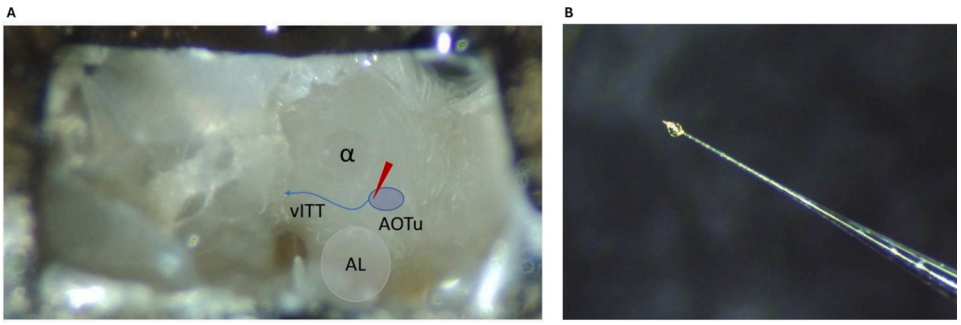


Fig. 2. (A) Window in the cuticula exposing the bee brain, with tracheae cleared on the right side. The injection site is indicated by a red arrow. The bee's antennae are facing downward. (B) Injection needle prepared with crystallized Fura at the tip.



Fig. 3. Bee head with antennae and mandibles immobilized using n-eicosane.

which corresponds to about 1 % of the intensity of the blue component in daylight. To minimize interference with fluorescence detection, the whole preparation was enclosed in a shielding structure made from rigid plastic foil painted black with acrylic paint (Fig. 4D). Two 473–488 nm notch filters (OD > 6.5, Chroma) were placed before the microscope's photomultiplier tubes to remove residual stray light. The laser power for stimulation was usually about 20 mW. Each experimental session comprised 15 trials with a 3–5 s visual stimulus and a 26 s inter-trial interval.

2.3. Magnetic stimulation setup

Magnetic fields were produced using a custom three-axis system of nested square Helmholtz coils (Fig. 6). The outermost coil pair was separated by 90 mm to accommodate nesting. The inner, middle, and outer coils had nominal widths of 154, 168, and 182 mm, with corresponding gaps of 75, 83, and 90 mm.

Field homogeneity was verified by simulation. Each coil comprised 26 windings of 1 mm copper wire distributed over five layers. Following Ahlers et al. [64], coils were double-wrapped, with two parallel windings per coil that could be electronically switched between series (field-adding) or series-opposition (field-cancelling) configurations. This allows a sham stimulation configuration to discriminate between genuine magnetic effects and electrical artifacts. A power supply (Rohde & Schwarz, NGE103) with remote control capability was used to generate fully customizable magnetic stimulus sequences.

To reduce electromagnetic interference, the coils were enclosed in a 1 cm thick aluminum housing providing radio-frequency shielding, supplemented with 0.5 mm μ-metal sheets (Holland Shielding) on the exterior to attenuate static magnetic fields. The small openings in the shield allow for minimal residual ambient fields, which were compensated for by the coil system. Under zero-field conditions, the residual magnetic field could be reduced to 1.3 mG, 0.2 mG, and 0.9 mG along the X, Y, and Z axes, respectively, with standard deviations of 0.7, 0.6, and 0.7 mG (Fig. 7).

Magnetic stimulation was generated, starting from a zero-field baseline, by applying a 0.5 G field along the X axis. To suppress high-frequency noise from abrupt current changes, the current was linearly ramped over 0.5 s (Fig. 8). The stimulus sequence for each trial involving magnetic stimulation was structured as follows: after a habituation time, first, the light was turned on for 13 s, followed by a 3 s magnetic stimulus, 10 s later also the light was switched off (Fig. 9). This sequence design allowed us from the light ON/OFF responses to evaluate if the AOTu remained responsive throughout each trial. The total trial duration was 52 s, and 10 trials were recorded per stimulation condition.

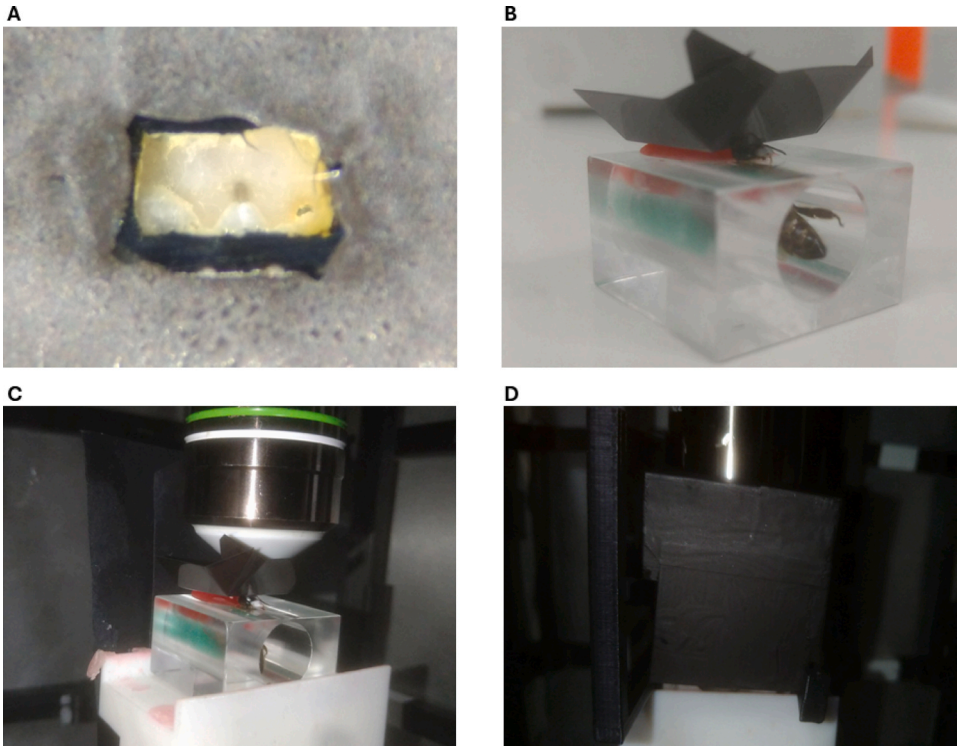


Fig. 4. (A) Bee brain visible through a transparent window in the painted plastic shield, (B) Fully prepared bee with a black plastic shield against stray light, (C) Prepared bee, positioned under the microscope objective. (D) Full stray light shielding added.

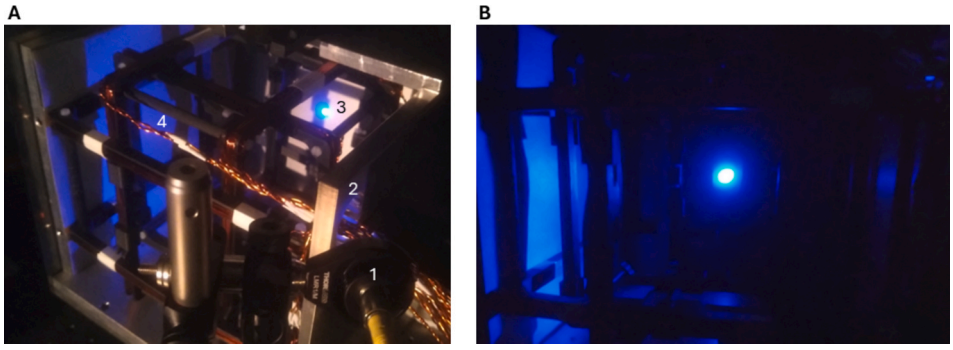


Fig. 5. Visual stimulation setup: (A) side view showing the laser path from the fiber output (1) through the hole in the shielding cage (2), scattered from the rear panel (3), and producing a homogeneous illumination of the side panel (4). (B) Front view showing the stimulus under experimental conditions. The illuminated left side panel covers the field of view of the bee's eye.

2.4. Calcium imaging

2.4.1. Microscopy setup

Calcium imaging was performed using a two-photon microscope (Ultima IV, Bruker) (Fig. 6) equipped with an ultra-short pulsed laser (Mai Tai DeepSee HP, Spectra-Physics). Excitation intensity was controlled by a Pockels cell, and scanning was performed with a pair of galvo mirrors. The microscope operated in epi-fluorescence configuration with a 20× water-immersion objective (NA 1.0, XLUMPLFLN20XW, Olympus). Emitted fluorescence was filtered with a 525±35 nm bandpass filter (Chroma) and detected by a photomultiplier tube (PH11706-40, Hamamatsu). The whole microscope is optically shielded from the environment by a light-tight enclosure.

2.4.2. Imaging parameters

The following image parameters yielded the best results, balancing spatial and temporal resolution with signal-to-noise ratio and photobleaching.

1) Imaging wavelength: An excitation wavelength of 780 nm maximized Fura fluorescence.
2) Laser power: The excitation laser power ranged from 4 to 5 mW, providing an optimal signal-to-noise ratio while minimizing photodamage, which was determined via the fluorescence signal decay over the entire experimental sequence.
3) Field of view: Given the approximate 120 μm width of the AOTu, images were acquired at 128×128 pixels with a 2×2 μm pixel size.
4) Exposure time: An exposure time of 6.4 μs per pixel provided a good signal-to-noise ratio while enabling recording at a 6 Hz frame rate.

The microscope data collection was triggered by the stimulus control computer, allowing for precise synchronisation between stimuli and recording.

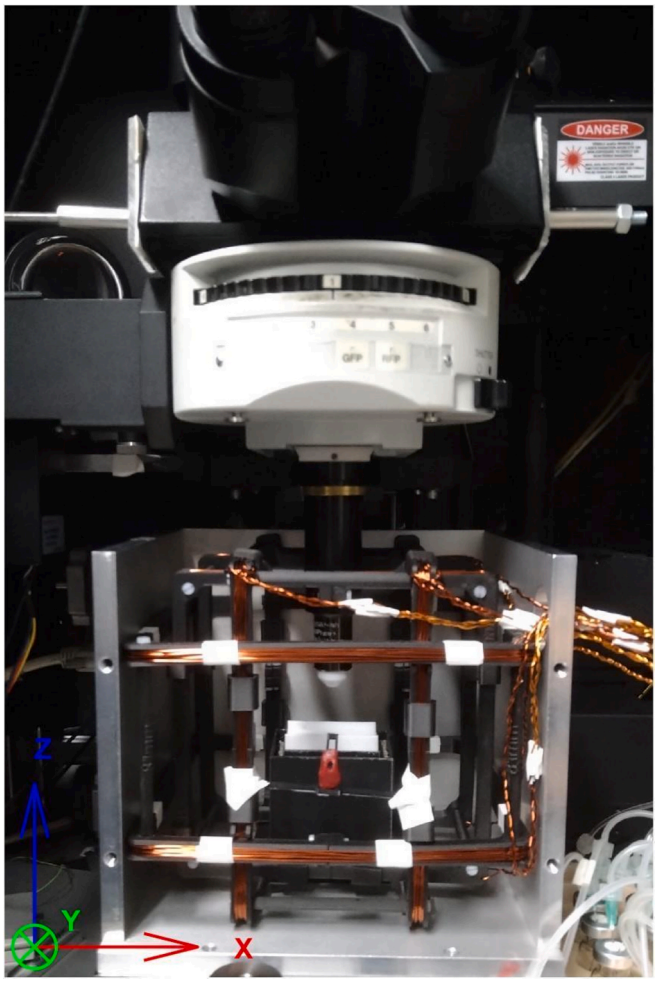


Fig. 6. Two-photon microscope with the coil assembly and the shielding cage, with the upper and front plates removed. The magnetic field axes are labeled at the bottom left.

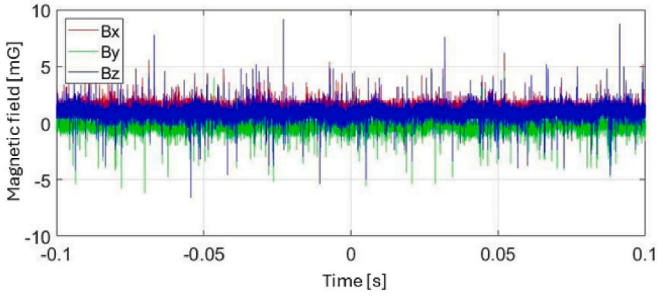


Fig. 7. Measurement of fluctuations and offset under zero magnetic field conditions at the center of the Helmholtz coils.

2.5. Data analysis

Two-photon calcium imaging data were analyzed with custom MATLAB scripts [65,66], directly after every experimental sequence, performing the following processing steps. The corresponding code is available on https://github.com/NeurophysicsTrento/BeeMagnetoreception.

2.5.1. Subjects

During development and testing of the experimental setup, approximately 200 bees were collected and prepared. Of these, approximately

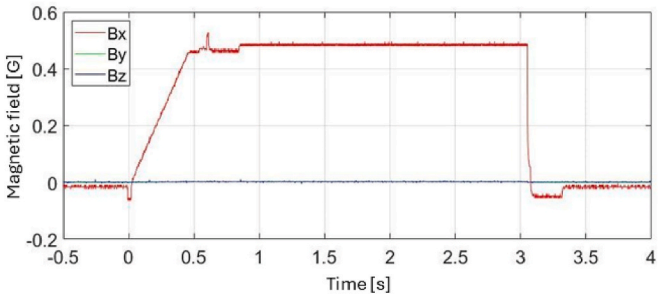


Fig. 8. Magnetic field measurement along the *X*-axis during a 3-second 0.5 G magnetic field stimulus with a 0.5-second ramp-up time.

90% survived overnight. Among the survivors, 80% were successfully stained, of which 50% exhibited visually evoked responses. But fewer than 10% of the bees exhibiting visually evoked responses also showed a reliable tonic response (see below). Approximately 80% of the visually responsive bees with a reliable tonic response showed apparent fluorescence changes around the magnetic-field onset. However, these changes were generally close to the detection limit and were often obscured by fluctuations, e.g. movement artefacts, precluding reliable quantitative analysis.

In the Results, we present one of the clearest examples of an apparent fluorescence change around magnetic-field onset. Additional recordings illustrating the variability across preparations are provided in the Supplementary Information.

2.5.2. Data analysis pipeline

1) Multi-frame TIFF files from sequential scans were combined into a single video for each experimental sequence, representing fluorescence intensity across space and time. The average intensity across the images over time was examined to evaluate photobleaching and the need for compensation. It also allowed to identify where motion artifacts or other fluctuations were dominating the signal, to eliminate these trials from further analysis.
2) The entire video sequence was averaged over time for a single reference image in which Regions of interest (ROIs) were selected. To assist this procedure, a regional homogeneity (ReHo) analysis can be performed, which highlights boundaries between regions of correlated signal fluctuations.
3) The fluorescence signal was then averaged within each ROI, which substantially increases the signal-to-noise ratio. Optional processing steps included detrending and high-pass filtering, both to compensate for the slow exponential decay due to photobleaching, and deconvolution with the Fura signal decay function to compensate for the delay due to unbinding of calcium from the detector molecule.
4) The relative fluorescence change was computed by normalizing the fluorescence during the stimulus with the average baseline during a pre-stimulus phase, usually lasting 5 s. Because neural activation decreases the Fura fluorescence intensity, traces were inverted so that activated neurons provided positive signal changes. The resulting measure, $-\Delta F/F$, is proportional to the neuronal firing rate [67], and we will in the following refer to this term as the calcium-response signal or simply the signal.
5) $-\Delta F/F$ was analyzed across the single trials, providing mean responses and standard deviations. ROIs were labeled as active when the mean calcium-response signal during the stimulus period was more than 1.96 × the pre-stimulus standard deviation, which corresponds to a 95% confidence threshold, visualized with blue-to-red shading. A proper statistical analysis was performed using paired *t*-tests between pre-, stimulus-, and post-stimulus periods, with false discovery rate (FDR) compensation.

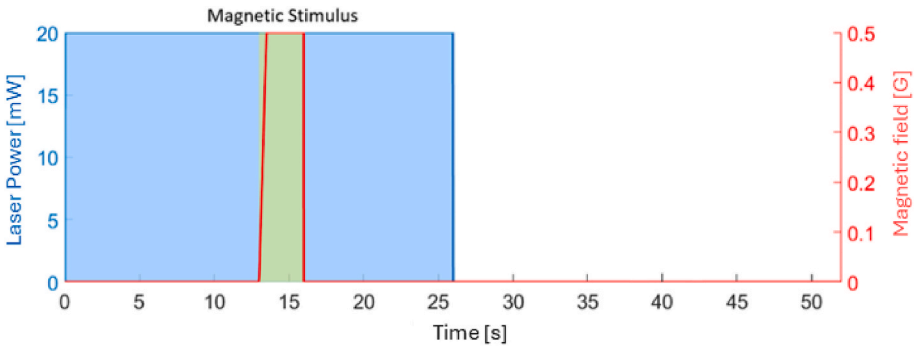


Fig. 9. Pulse sequences for the magnetic response experiment, including visual (blue) and magnetic (red) stimuli. Magnetic field strength and blue laser power at the fiber output are indicated.

3. Results

3.1. Structural data

Mosaicking two images acquired with a 20× objective enables visualization of the dye diffusion pathway from the injection side near the left AOT along the ventral inter-tubercle tract (vlTT) to the contralateral AOTu (Fig. 10).

For each subject, the volumetric structure of the AOTu was determined by recording Z-stacks at higher resolution after the functional imaging sequence, using 512×512-pixel images and a slice distance of 2.5 µm (Fig. 11). These data enable 3D reconstruction using magic wand image segmentation in Amira (V5.4, Thermo Scientific) (Fig. 11B).

3.2. Light-sensitive responses

A typical AOTu response to the described visual stimulus is shown in Fig. 12A. It displays temporal dynamics consistent with previous reports [61,68]. The calcium trace exhibits two peaks, an ON response at stimulus onset and an OFF response at the offset, as well as a lower tonic response during illumination. The calcium-response signal for the ON and OFF responses reached 0.8% and 1.1%, respectively, with a tonic component of 0.5%, which is lower than previous widefield microscopy results (ON: 4%, OFF: 5%, tonic: 4%) [60]. This reduction is likely due to the thinner optical sectioning provided by two-photon microscopy.

Signal background changes due to the visual stimulus (Fig. 12B) were quantified in a region posterior to the AOTu (Fig. 12C, ROI 2) without significant fluorescence, revealing a 0.3% decrease in $-\Delta F/F$ due to the laser light despite extensive mechanical and optical shielding. This background attenuated the apparent AOTu response amplitude, thus its precise value remains uncertain. Consequently, 0.3% was chosen as the upper limit for acceptable background change, constraining the maximum laser intensity used for visual stimulation.

3.3. Exploratory recording during magnetic stimulation

Calcium-response signal recordings from a bee subjected to the magnetic stimulation protocol after piecewise linear detrending are shown in Fig. 13A. Distinct visual ON and OFF responses remain clearly detectable. The tonic component was transiently suppressed after the on-response, and reemerged after approximately 2-3 s. At magnetic field onset, the signal initially increased by about 0.2% within the first second and decayed with a similar time constant as the visual responses.

After the magnetic field offset, the signal returned to its pre-stimulus baseline. An exploratory paired *t*-test comparing the pre-stimulus and stimulus-period signals across ten repeated trials from this single subject yielded $p = 0.13$.

Further examples for bees with potential signal changes at the

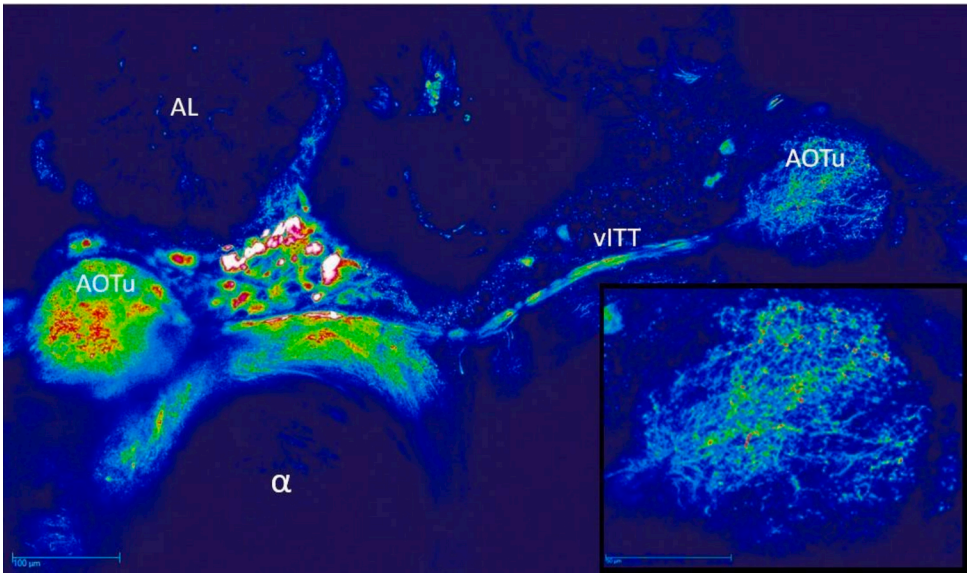


Fig. 10. Image of the bee brain showing staining, with the bottom-right inset providing a zoomed view of the AOTu. The injection site is located in the left AOTu, with dye diffusing to the right AOTu via the vlTT. The dimensions of the full image are 425 × 240 µm^2, and of the inset 160 × 115 µm^2. Abbreviations: AL: antennal lobe; α: mushroom body α-lobe; vlTT: ventral inter-tubercle tract.

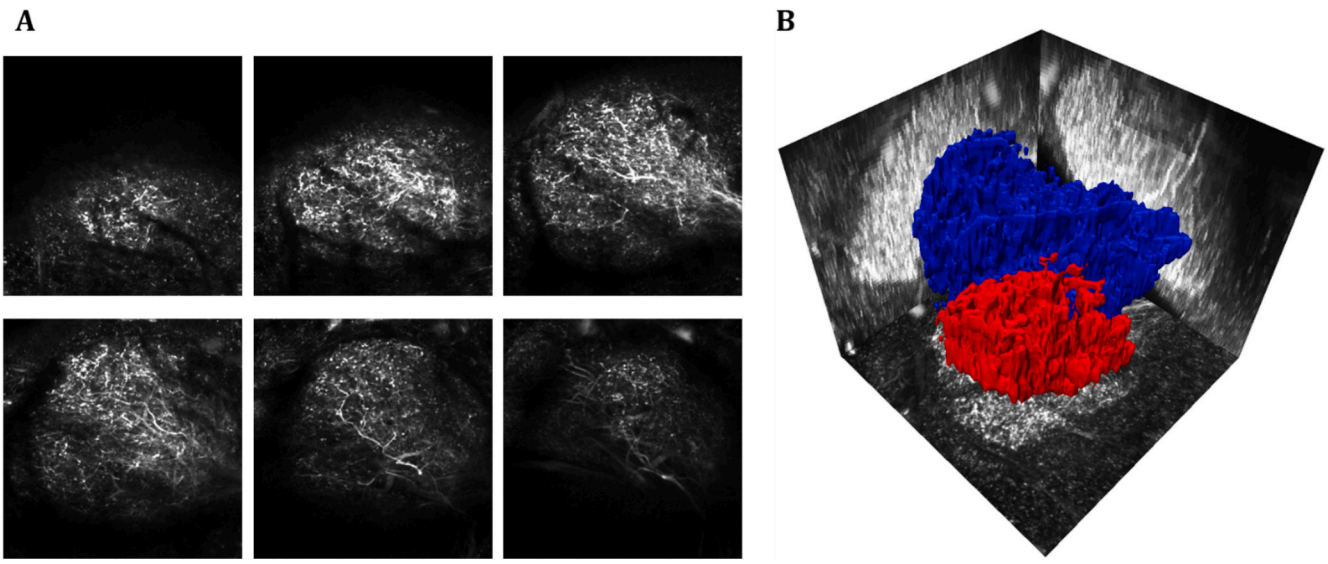


Fig. 11. (A) Stack of images traversing the AOTu, image dimensions are 160 × 160 μm^2, and the distance between the shown images is 20 μm. (B) Reconstructed 3D structure of the same AOTu with the ventral lobe below and the dorsal lobe above, image dimensions are 160 × 160 × 140 μm^3.

magnetic field stimulus onset, although even closer to the detection limit, are shown in the Supplementary information (Fig. S1-S3).

4. Discussion

Several parameters were critical for obtaining reliable AOTu visual responses, including two-photon excitation power, visual stimulus intensity, and the imaging plane. The excitation power had to be carefully adjusted: While increasing the power amplified the fluorescence and reduced the relative background from the visual stimulus, it also amplified the noise and the photobleaching. Minor changes in the excitation laser power on the order of 0.2 mW were decisive for whether weak ON/OFF responses were visible, the signal was masked by noise (if the power was too high), or stimulus light artifacts dominated (if the power was too low). Using optimal laser intensities, peak AOTu activation signals of 1.2% were obtained. The imaging plane also affected response amplitude, with the most robust signals recorded 10 μm above the AOTu center.

Although parameters that yield pronounced ON and OFF responses were relatively straightforward to identify, obtaining a clear tonic component during stimulation proved substantially more challenging and depended critically on overall preparation quality, being highly sensitive to both dye loading and tissue integrity. Because the AOTu lies close to the brain surface, it was particularly vulnerable to damage during tracheal removal, and even minor, visually undetected damage frequently abolished the tonic response. In such cases, otherwise well-stained tubercles often exhibited only ON/OFF responses or no detectable activity at all.

Dye concentration imposed an additional constraint: insufficient staining increased noise due to dominant background autofluorescence, whereas excessive staining often eliminated detectable activity. In heavily stained tubercles, reducing excitation power to compensate for elevated baseline fluorescence did not restore robust responses, and at most, a sharp ON response was observed. This loss of signal may reflect excessive intracellular buffering by the calcium indicator Fura, attenuating activity-dependent calcium transients and thereby suppressing detectable responses [69].

The injection strategy also proved important: using three injections with borosilicate glass needles, each containing a small amount of dye, was preferable to a single injection with the same total dye load, because the latter often caused leakage into adjacent regions, such as the mushroom bodies, and increased background fluorescence. In contrast, three small injections at the same location limited background staining while still providing sufficient labeling of the tubercle.

To reliably detect a response to magnetic stimulation, a strong and stable visual response was required, characterized in particular by a high tonic response with low noise. If the experimental parameters were not optimized so that the bee did not exhibit sustained visual activity, no detectable change was observed during magnetic stimulation. As the calcium-response signal during magnetic stimulation manifested as a decrease, the response suggests that this type of magnetic stimulus may suppress neural activity. Thus, the larger the visual response, the better the detectability of this inhibitory change.

The origin of this potential inhibition in brain activity in response to the magnetic stimulus remains to be determined, but RPM models indeed suggest a bright/dark modulation of the blue-light photoreceptor activity that is projected via the optic lobe into the AOTu [45]. Whether the AOTu can also show excitation in response to magnetic stimuli of different orientations remains to be investigated.

The magnetic stimulus used here was an initial feasibility stimulus designed to determine whether measurable fluorescence modulation could be detected during operation of the coil system. Because it involved a change from a near-zero field to 0.5 G, it neither reproduced the magnetic cues normally experienced by honey bees nor directly tested the defining predictions of the radical-pair mechanism. Future experiments should therefore rotate the direction of an Earth-strength magnetic field while maintaining constant intensity and compare responses under blue light, red light, and darkness. Active magnetic stimulation should additionally be compared with field-cancelling sham stimulation, which reproduces the electrical stimulation sequence without generating a magnetic-field change. The three-axis, double-wrapped coil system was designed to support all these protocols.

In the analyzed bee with the magnetic pulse sequence, the tonic response to the visual stimulus during the magnetic pulse sequence initially dropped back toward pre-stimulus levels after the ON response and recovered after 2–3 s (Fig. 13A). This reduction was never observed with the pure visual stimulus sequence (Fig. 12A), and its origin remains unclear. The only systematic difference between the two stimulus protocols is that the magnetic sequence begins in a zero-field environment, suggesting that the AOTu responds differently to pure optical stimuli under hypomagnetic field conditions. However, this interpretation still requires confirmation via sham stimulation control.

The apparent fluorescence modulation shown in Fig. 13 must be interpreted cautiously. All ten trials were obtained from a single bee and

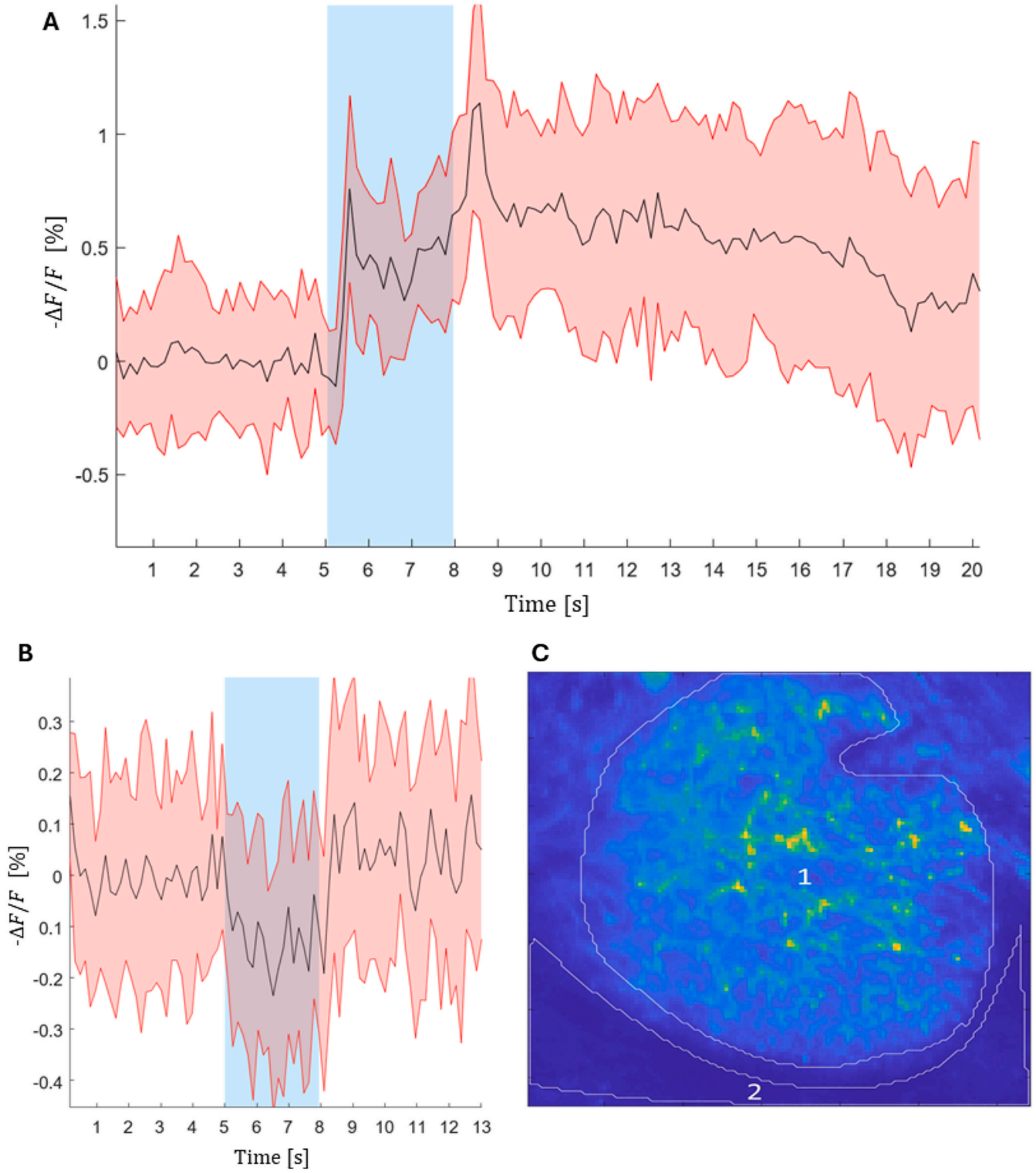


Fig. 12. Time series of Fura calcium-response signal during the visual stimulus sequence, showing the percentual change averaged over 15 trials in a single subject. (A) Calcium- response of the AOTu to the stimulus (ROI1). (B) Calcium-response signal in the background region under the same stimulus (ROI2). (C) Total fluorescence intensity image averaged across all frames, from which ROI1 and ROI2 were chosen. ROI1 shows the AOTu, where signal values were measured. ROI2 represents a reference area where total fluorescence is minimal, to determine the background signal from the visual stimulation light. Red curves indicate a significant change in fluorescence from the pre-stimulus baseline (95% confidence threshold).

therefore characterize only trial-to-trial variability within that individual; they do not constitute independent biological replicates. The exploratory comparison was not statistically significant and cannot support inference across bees. Consequently, the observed transient should not be regarded as evidence for a magnetically mediated neural response. Rather, this recording illustrates the application of the combined imaging and stimulation protocol, as well as its current limitations in resolving small signal changes.

It is also important to assess whether the magnetic response is influenced by the visual stimulus protocol, specifically whether the

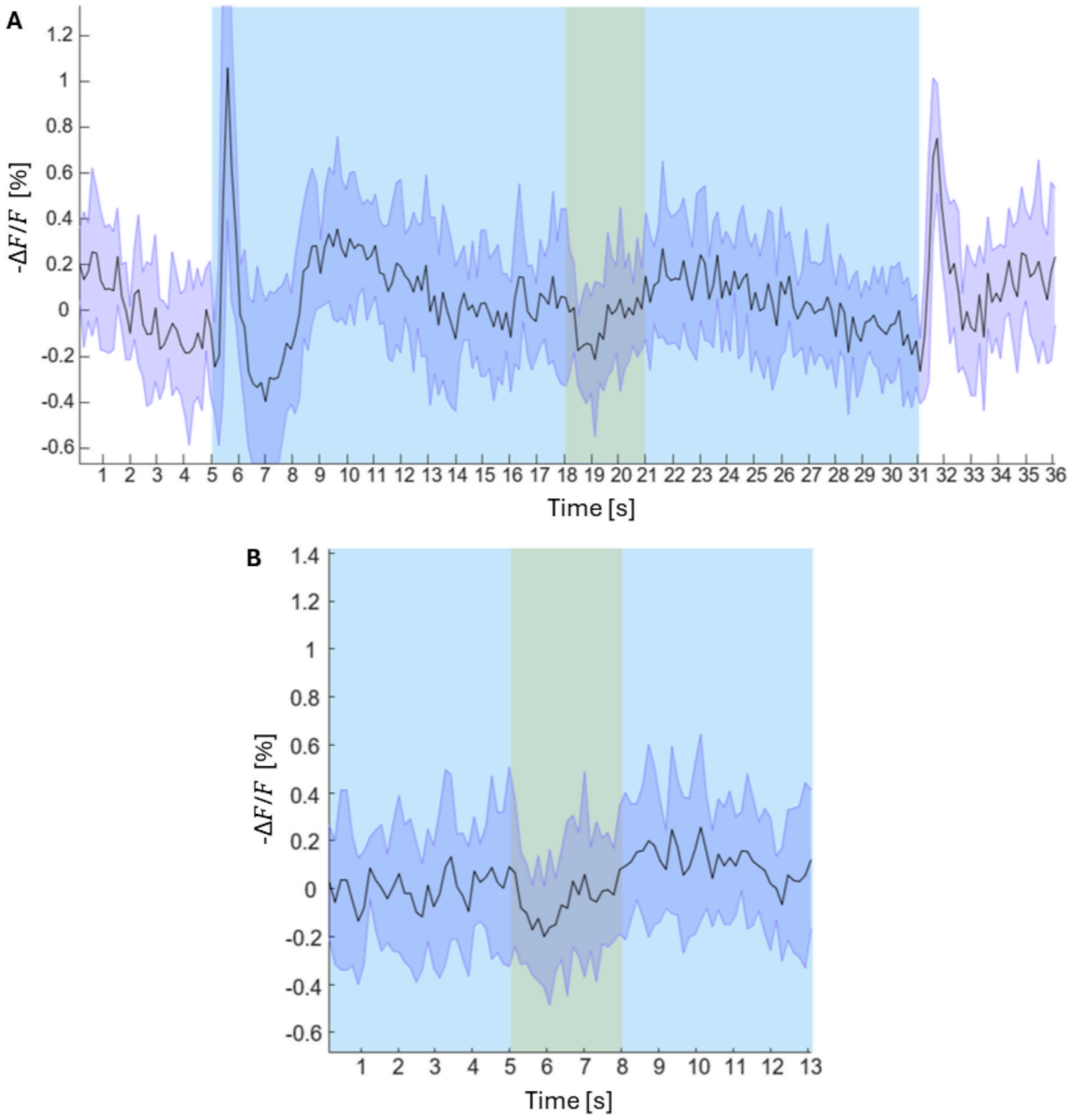


Fig. 13. Detrended time-series recordings of calcium-response signal in the AOTu during magnetic stimulation averaged over 10 trials. (A) Response of the AOTu over the full stimulus sequence. (B) Response of the AOTu to the magnetic stimulus, in the same recording.

visual stimulus remains on across trials or alternates on and off during each trial. So far, only the latter has been tested (Fig. 9) to confirm that the AOTu remained equally responsive to visual stimuli during each trial.

5. Conclusion and outlook

The weak and variable nature of magnetic-field-dependent responses, which has made controlled experimental investigation particularly challenging across model systems [70], has also limited our study to largely qualitative results. However, this two-photon imaging approach presented here suggests the feasibility of detecting weak, magnetic-field-dependent modulation of neural activity in the honeybee brain. By enabling *in vivo* measurements in a higher-order visual processing region, this framework provides access to downstream neural circuits in which magnetically elicited signals may be integrated and amplified. The observation of small fluorescence changes in the AOTu may provide a basis for probing the neural correlates of magnetoreception beyond primary sensory structures.

Several technical improvements are expected to further enhance sensitivity and interpretability. The approximately 0.3% change associated with the blue-light background is comparable in magnitude to the apparent 0.2% change observed during magnetic stimulation. Although normalization during continuous illumination corrects for the static light-induced offset, it cannot remove temporal fluctuations in the scattered-light background, which may obscure or mimic fluorescence changes of this magnitude. We therefore plan to implement a flyback stimulation protocol, in which the blue-light stimulus is delivered only during the galvanometric scanner retrace, when fluorescence data are not acquired. By temporally separating visual stimulation from fluorescence detection, this approach should prevent direct detection of scattered blue light and permit higher stimulus intensities without

increasing the recorded optical background [71].

The present measurements are also restricted to a single imaging plane, whereas magnetically modulated activity is likely distributed across the three-dimensional structure of the AOTu. Extending the approach to volumetric imaging will allow reconstruction of spatial activity patterns and may reveal localized or distributed response motifs.

While the present results provide no evidence of magnetosensitive responses, the setup will allow for further investigation of the underlying mechanism, in particular, a controlled testing of key predictions of the radical pair mechanism models, including the requirement for short-wavelength (blue) light, the expected sensitivity to magnetic field axis rather than polarity, and the disruption of responses by weak radio-frequency fields, which can be easily integrated into the setup. Systematic variation of these parameters will be essential to determine whether the observed signals are consistent with a radical-pair–based mechanism.

The first signals highlight the importance of systematically linking stimulus design to underlying biological hypotheses. In particular, the predominance of inhibitory responses under the present conditions complicates the interpretation of light dependence and means that a dark conditions control cannot be applied directly to the current response, which was observed relative to blue-light-evoked excitation. Alternative magnetic-field configurations are therefore being investigated to elicit excitatory responses that can be compared under blue light and dark conditions. Identifying such conditions will be critical for disentangling the contributions of visual processing and magnetically induced modulation.

Beyond the visual pathway hypothesis, there are alternative hypotheses to be investigated. Iron-containing abdominal tissues and signal transmission through the ventral nerve cord (VNC) have previously been implicated in honey bee magnetoreception [23–26], although neither the receptor cells nor their central projections have been established [23–26]. A potential test for this hypothesis could be the imaging of neuropils where these signals might be integrated with other inputs, like the optically accessible mushroom body calyces. Combined with a manipulation of the VNC [25], this approach could test whether putative abdomen-derived magnetic information reaches the central brain. Also, the hypothesis that receptors on the antennae might be involved in magnetoreception is testable with our setup, as antennal lobes are easy to image. The most universal approach would be staining all neurons at once, which was already achieved in bees by pan-neuronal expression of a genetically encoded calcium sensor [52].

Overall, this imaging framework provides a new methodological approach for studying magnetoreception within intact neural circuits, bridging the gap between molecular models and systems-level function. By enabling controlled, *in vivo* imaging of weak magnetic effects in the brain, it may open new avenues for testing mechanistic hypotheses and for dissecting how magnetic and visual information are integrated in the neural circuitry underlying animal navigation.

CRediT authorship contribution statement

Alan Oesterle: Data curation, Formal analysis, Investigation, Methodology, Software, Validation, Visualization, Writing – original draft, Writing – review & editing. **Alara Kiriş:** Methodology, Investigation, Writing – review & editing. **Albrecht Haase:** Conceptualization, Funding acquisition, Methodology, Project administration, Resources, Software, Supervision, Validation, Visualization, Writing – original draft, Writing – review & editing.

Declaration of competing interest

The authors declare that they have no known competing financial interests or personal relationships that could have appeared to influence the work reported in this paper.

Acknowledgements

We acknowledge help with the magnetic field simulation by Riccardo Cabassi. A.O. acknowledges financial support from the Q@TN joint laboratory.

Appendix A. Supplementary data

Supplementary data to this article can be found online at https://doi.org/10.1016/j.ymeth.2026.09.005.

Data availability

Data will be made available on request.

References

[1] N. Lambert, Y.-N. Chen, Y.-C. Cheng, C.-M. Li, G.-Y. Chen, F. Nori, Quantum biology, Nat. Phys. 9 (2013) 10–18, https://doi.org/10.1038/nphys2474.
[2] W. Wiltschko, R. Wiltschko, Magnetic compass of european robins, Science 176 (1972) (1979) 62–64, https://doi.org/10.1126/science.176.4030.62.
[3] J. Olcese, S. Reuss, P. Semm, Geomagnetic field detection in rodents, Life Sci. 42 (1988) 605–613, https://doi.org/10.1016/0024-3205(88)90451-1.
[4] N.F. Putman, P. Verley, C.S. Endres, K.J. Lohmann, Magnetic navigation behavior and the oceanic ecology of young loggerhead sea turtles, J. Exp. Biol. 218 (2015) 1044–1050, https://doi.org/10.1242/jeb.109975.
[5] J.B. Phillips, O. Sayeed, Wavelength-dependent effects of light on magnetic compass orientation in Drosophila melanogaster, J. Comp. Physiol. A 172 (1993) 303–308, https://doi.org/10.1007/BF00216612.
[6] J.B. Anderson, R.K. Vander Meer, Magnetic orientation in the fire ant, Solenopsis invicta, Naturwissenschaften 80 (1993) 568–570, https://doi.org/10.1007/BF01149274.
[7] R.B. Srygley, R. Dudley, E.G. Oliveira, A.J. Riveros, Experimental evidence for a magnetic sense in neotropical migrating butterflies (Lepidoptera: Pieridae), Anim. Behav. 71 (2006) 183–191, https://doi.org/10.1016/j.anbehav.2005.04.013.
[8] M. Vácha, Laboratory behavioural assay of insect magnetoreception: Magnetosensitivity of Periplaneta americana, J. Exp. Biol. 209 (2006) 3882–3886, https://doi.org/10.1242/jeb.02456.
[9] K.J. Lohmann, N.D. Pentcheff, G.A. Nevitt, G.D. Stetten, R.K. Zimmer-Faust, H. E. Jarrard, L.C. Boles, Magnetic orientation of spiny lobsters in the ocean: experiments with undersea coil systems, J. Exp. Biol. 198 (1995) 2041–2048, https://doi.org/10.1242/jeb.198.10.2041.
[10] S. Nimpf, D.A. Keays, Myths in magnetosensation, IScience 25 (2022) 104454, https://doi.org/10.1016/j.isci.2022.104454.
[11] M. Beekman, F.L.W. Ratnieks, Long-range foraging by the honey-bee, Apis mellifera L, Funct. Ecol. 14 (2000) 490–496, https://doi.org/10.1046/j.1365-2435.2000.00443.x.
[12] S. Rossel, R. Wehner, How bees analyse the polarization patterns in the sky - Experiments and model, J. Comp. Physiol. A 154 (1984) 607–615, https://doi.org/10.1007/BF01350213.
[13] T.S. Collett, J. Baron, Biological compasses and the coordinate frame of landmark memories in honeybees, Nature 368 (1994) 137–140, https://doi.org/10.1038/368137a0.
[14] J.F. Cheeseman, C.D. Millar, U. Greggers, K. Lehmann, M.D.M. Pawley, C. R. Gallistel, G.R. Warman, R. Menzel, Way-finding in displaced clock-shifted bees proves bees use a cognitive map, in: Proceedings of the National Academy of Sciences 111, 2014, pp. 8949–8954, https://doi.org/10.1073/pnas.1408039111.
[15] M. Lindauer, H. Martin, Magnetic effect on dancing bees, Symposium NASA SP-262, Animal Orientation and Navigation (1972) 559–567.
[16] J.L. Gould, J.L. Kirschvink, K.S. Deffeyes, Bees have magnetic remanence, Science 201 (1978) (1979) 1026–1028, https://doi.org/10.1126/science.201.4360.1026.
[17] M.M. Walker, M.E. Bitterman, Honeybees can be trained to respond to very small changes in geomagnetic field intensity, J. Exp. Biol. 145 (1989) 489–494, https://doi.org/10.1242/jeb.145.1.489.
[18] D.E. Schmitt, H.E. Esch, Magnetic orientation of honeybees in the laboratory, Naturwissenschaften 80 (1993) 41–43, https://doi.org/10.1007/BF01139759.
[19] V. Lambinet, M.E. Hayden, C. Reid, G. Gries, Honey bees possess a polarity-sensitive magnetoreceptor, J. Comp. Physiol. A 203 (2017) 1029–1036, https://doi.org/10.1007/s00359-017-1214-4.
[20] P. Migdał, E. Berbeć, P. Bieńkowski, M. Plotnik, A. Murawska, K. Latarowski, Exposure to magnetic fields changes the behavioral pattern in honeybees (Apis mellifera L.) under laboratory conditions, Animals 12 (2022), https://doi.org/10.3390/ani12070855.
[21] T. Válková, M. Vácha, How do honeybees use their magnetic compass? Can they see the North? Bull. Entomol. Res. 102 (2012) 461–467, https://doi.org/10.1017/S0007485311000824.
[22] R. Brandt, T. Rohlfing, J. Rybak, S. Krofczik, A. Maye, M. Westerhoff, H.C. Hege, R. Menzel, Three-dimensional average-shape atlas of the honeybee brain and its applications, J. Comp. Neurol. 492 (2005) 1–19, https://doi.org/10.1002/cne.20644.

[23] J.A. Shaw, A. Boyd, M. House, G. Cowin, B. Baer, Multi-modal imaging and analysis in the search for iron-based magnetoreceptors in the honeybee Apis mellifera, R. Soc. Open Sci. 5 (2018) 181163, https://doi.org/10.1098/rsos.181163.
[24] C.Y. Hsu, F.Y. Ko, C.W. Li, K. Fann, J.T. Lue, Magnetoreception system in honeybees (Apis mellifera), PLoS One 2 (2007), https://doi.org/10.1371/journal.pone.0000395.
[25] C.H. Liang, C.L. Chuang, J.A. Jiang, E.C. Yang, Magnetic sensing through the abdomen of the honey bee, Sci. Rep. 6 (2016) 1–7, https://doi.org/10.1038/srep23657.
[26] V. Lambinet, M.E. Hayden, K. Reigl, S. Gomis, G. Gries, Linking magnetite in the abdomen of honey bees to a magnetoreceptive function, in: Proceedings of the Royal Society B: Biological Sciences 284, 2017, https://doi.org/10.1098/rspb.2016.2873.
[27] O. Bazalova, M. Kvicalova, T. Valkova, P. Slaby, P. Bartos, R. Netusil, K. Tomanova, P. Braeunig, H.-J. Lee, I. Sauman, M. Damulewicz, J. Provaznik, R. Pokorny, D. Dolezel, M. Vacha, Cryptochrome 2 mediates directional magnetoreception in cockroaches, Proc. Natl. Acad. Sci. 113 (2016) 1660–1665, https://doi.org/10.1073/pnas.1518622113.
[28] G. Wan, A.N. Hayden, S.E. Iiams, C. Merlin, Cryptochrome 1 mediates light-dependent inclination magnetosensing in monarch butterflies, Nat. Commun. 12 (2021) 771, https://doi.org/10.1038/s41467-021-21002-z.
[29] P.J. Hore, H. Mouritsen, The radical-pair mechanism of magnetoreception, Annu. Rev. Biophys. 45 (2016) 299–344, https://doi.org/10.1146/annurev-biophys-032116-094545.
[30] S. Johnsen, K.J. Lohmann, The physics and neurobiology of magnetoreception, Nat. Rev. Neurosci. 6 (2005) 703–712, https://doi.org/10.1038/nrn1745.
[31] R. Blakemore, Magnetotactic bacteria, Science 190 (1975) (1979) 377–379, https://doi.org/10.1126/science.170679.
[32] J.L. Kirschvink, J.L. Gould, Biogenic magnetite as a basis for magnetic field detection in animals, Biosystems 13 (1981) 181–201, https://doi.org/10.1016/0303-2647(81)90060-5.
[33] A.J. Kalmijn, Electric and magnetic field detection in elasmobranch fishes, Science 218 (1982) (1979) 916–918, https://doi.org/10.1126/science.7134985.
[34] K. Schulten, Magnetic field effects in chemistry and biology, in: Festkörperprobleme 22, Springer Berlin Heidelberg, Berlin, Heidelberg, 1982: pp. 61–83. https://doi.org/10.1007/BFb0107935.
[35] T. Ritz, S. Adem, K. Schulten, A model for photoreceptor-based magnetoreception in birds, Biophys. J . 78 (2000) 707–718, https://doi.org/10.1016/S0006-3495(00)76629-X.
[36] P.J. Hore, A hybrid compass mechanism combining radical pairs and magnetite crystals, Proc. Natl. Acad. Sci. 123 (2026) 2017. https://doi.org/10.1073/pnas.2524093123.
[37] K.M. Goforth, C.M.F. Lohmann, A. Gavin, R. Henning, A. Harvey, T.L. Hinton, D. S. Lim, K.J. Lohmann, Learned magnetic map cues and two mechanisms of magnetoreception in turtles, Nature 638 (2025) 1015–1022, https://doi.org/10.1038/s41586-024-08554-y.
[38] G.C. Nordmann, S.D. Balay, T.N. Kapuruge, M. Numi, C. Leeb, S. Nimpf, E. P. Malkemper, L. Landler, D.A. Keays, A global screen for magnetically induced neuronal activity in the pigeon brain, Science 6425 (2025) (1979) 1–10, https://doi.org/10.1126/science.aea6425.
[39] T. Ritz, P. Thalau, J.B. Phillips, R. Wiltschko, W. Wiltschko, Resonance effects indicate a radical-pair mechanism for avian magnetic compass, Nature 429 (2004) 177–180, https://doi.org/10.1038/nature02534.
[40] H. Mouritsen, U. Janssen-Bienhold, M. Liedvogel, G. Feenders, J. Stalleicken, P. Dirks, R. Weiler, Cryptochromes and neuronal-activity markers colocalize in the retina of migratory birds during magnetic orientation, in: Proceedings of the National Academy of Sciences 101, 2004, pp. 14294–14299, https://doi.org/10.1073/pnas.0405968101.
[41] R.J. Gegear, A. Casselman, S. Waddell, S.M. Reppert, Cryptochrome mediates light-dependent magnetosensitivity in Drosophila, Nature 454 (2008) 1014–1018, https://doi.org/10.1038/nature07183.
[42] L.E. Foley, R.J. Gegear, S.M. Reppert, Human cryptochrome exhibits light-dependent magnetosensitivity, Nat. Commun. 2 (2011) 353–356, https://doi.org/10.1038/ncomms1364.
[43] J. Xu, L.E. Jarocha, T. Zollitsch, M. Konowalczyk, K.B. Henbest, S. Richert, M. J. Golesworthy, J. Schmidt, V. Déjean, D.J.C. Sowood, M. Bassetto, J. Luo, J. R. Walton, J. Fleming, Y. Wei, T.L. Pitcher, G. Moise, M. Herrmann, H. Yin, H. Wu, R. Bartölke, S.J. Käsehagen, S. Horst, G. Dautaj, P.D.F. Murton, A.S. Gehrckens, Y. Chelliah, J.S. Takahashi, K.W. Koch, S. Weber, I.A. Solov'yov, C. Xie, S. R. Mackenzie, C.R. Timmel, H. Mouritsen, P.J. Hore, Magnetic sensitivity of cryptochrome 4 from a migratory songbird, Nature 594 (2021) 535–540, https://doi.org/10.1038/s41586-021-03618-9.
[44] J.B. Phillips, R. Muheim, P.E. Jorge, A behavioral perspective on the biophysics of the light-dependent magnetic compass: a link between directional and spatial perception? J. Exp. Biol. 213 (2010) 3247–3255, https://doi.org/10.1242/jeb.020792.
[45] I.A. Solov'yov, H. Mouritsen, K. Schulten, Acuity of a cryptochrome and vision-based magnetoreception system in birds, Biophys. J. 99 (2010) 40–49, https://doi.org/10.1016/j.bpj.2010.03.053.
[46] M. Vacha, Magnetoreception of Invertebrates (2017), https://doi.org/10.1093/oxfordhb/9780190456757.013.16.
[47] H. Mouritsen, Long-distance navigation and magnetoreception in migratory animals, Nature 558 (2018) 50–59, https://doi.org/10.1038/s41586-018-0176-1.
[48] A.Y. Rotov, A.A. Goriachenkov, R.V. Cherbunin, M.L. Firsov, N. Chernetsov, L. A. Astakhova, Magnetoreceptory function of european robin retina: electrophysiological and morphological non-homogeneity, Cells 11 (2022) 3056, https://doi.org/10.3390/cells11193056.
[49] A.A. Bradlaugh, G. Fedele, A.L. Munro, C.N. Hansen, J.M. Hares, S. Patel, C. P. Kyriacou, A.R. Jones, E. Rosato, R.A. Baines, Essential elements of radical pair magnetosensitivity in Drosophila, Nature 615 (2023) 111–116, https://doi.org/10.1038/s41586-023-05735-z.
[50] K. Svoboda, R. Yasuda, Principles of two-photon excitation microscopy and its applications to neuroscience, Neuron 50 (2006) 823–839, https://doi.org/10.1016/j.neuron.2006.05.019.
[51] A. Haase, E. Rigosi, F. Trona, G. Anfora, G. Vallortigara, R. Antolini, C. Vinegoni, In-vivo two-photon imaging of the honey bee antennal lobe, Biomed. Opt. Express 2 (2011) 131, https://doi.org/10.1364/BOE.2.000131.
[52] J. Carcaud, M. Otte, B. Grünewald, A. Haase, J.-C. Sandoz, M. Beye, Multisite imaging of neural activity using a genetically encoded calcium sensor in the honey bee, PLoS Biol. 21 (2023) e3001984, https://doi.org/10.1371/journal.pbio.3001984.
[53] F. Helmchen, W. Denk, Deep tissue two-photon microscopy, Nat. Methods 2 (2005) 932–940, https://doi.org/10.1038/nmeth818.
[54] M. Oheim, E. Beaurepaire, E. Chaigneau, J. Mertz, S. Charpak, Two-photon microscopy in brain tissue: parameters influencing the imaging depth, J. Neurosci. Methods 111 (2001) 29–37, https://doi.org/10.1016/S0165-0270(01)00438-1.
[55] M. Andrione, B.F. Timberlake, G. Vallortigara, R. Antolini, A. Haase, Morphofunctional experience-dependent plasticity in the honeybee brain, Learn. Mem. 24 (2017) 622–629, https://doi.org/10.1101/lm.046243.117.
[56] E. Tiraboschi, L. Leonardelli, G. Segata, A. Haase, Parallel processing of olfactory and mechanosensory information in the honey bee antennal lobe, 2021.05.11.443598, Front. Physiol. 12 (2021), https://doi.org/10.3389/fphys.2021.790453.
[57] S. Moguilner, E. Tiraboschi, G. Fantoni, H. Strelevitz, H. Soleimani, L. Del Torre, U. Hasson, A. Haase, Neuronal correlates of sleep in honey bees, Neural Netw. 189 (2025) 107575, https://doi.org/10.1016/j.neunet.2025.107575.
[58] R. Menzel, M. Blakers, Colour receptors in the bee eye - Morphology and spectral sensitivity, J. Comp. Physiol. A 108 (1976) 11–13, https://doi.org/10.1007/BF00625437.
[59] U. Homberg, S. Heinze, K. Pfeiffer, M. Kinoshita, B. el Jundi, Central neural coding of sky polarization in insects, Philos. Trans. R. Soc., B 366 (2011) 680–687, https://doi.org/10.1098/rstb.2010.0199.
[60] T. Mota, N. Yamagata, M. Giurfa, W. Gronenberg, J.-C. Sandoz, Neural organization and visual processing in the anterior optic tubercle of the honeybee brain, J. Neurosci. 31 (2011) 11443–11456, https://doi.org/10.1523/JNEUROSCI.0995-11.2011.
[61] T. Mota, W. Gronenberg, M. Giurfa, J.C. Sandoz, Chromatic processing in the anterior optic tubercle of the honey bee brain, J. Neurosci. 33 (2013) 4–16, https://doi.org/10.1523/JNEUROSCI.1412-12.2013.
[62] M. Held, A. Berz, R. Hensgen, T.S. Muenz, C. Scholl, W. Rössler, U. Homberg, K. Pfeiffer, Microglomerular synaptic complexes in the sky-compass network of the honeybee connect parallel pathways from the anterior optic tubercle to the central complex, Front. Behav. Neurosci. 10 (2016) 1–15, https://doi.org/10.3389/fnbeh.2016.00186.
[63] M. Paoli, M. Andrione, A. Haase, Imaging Techniques in Insects, in: L.J. Rogers, G. Vallortigara (Eds.), Lateralized Brain Functions: Methods in Human and Non-Human Species, 1st ed.,, Springer, New York, New York, NY, 2017, pp. 471–519, https://doi.org/10.1007/978-1-4939-6725-4_15.
[64] M.T. Ahlers, C.T. Block, M. Winklhofer, M. Greschner, Integration and evaluation of magnetic stimulation in physiology setups, PLoS One 17 (2022) e0271765, https://doi.org/10.1371/journal.pone.0271765.
[65] E. Tiraboschi, L. Minati, S. Monachino, M. Frasca, A. Haase, Transfer function-based characterization of the honey bee olfactory system: from biology to electronic circuits, IEEE Access 10 (2022) 17169–17188, https://doi.org/10.1109/ACCESS.2022.3149822.
[66] M. Paoli, N. Weisz, R. Antolini, A. Haase, Spatially resolved time-frequency analysis of odour coding in the insect antennal lobe, Eur. J. Neurosci. 44 (2016) 2387–2395, https://doi.org/10.1111/ejn.13344.
[67] L. Moreaux, G. Laurent, Estimating firing rates from calcium signals in locust projection neurons in vivo, Front. Neural Circuits 1 (2007) 2, https://doi.org/10.3389/neuro.04.002.2007.
[68] T. Mota, B. Paffhausen, R. Menzel, Chromatic processing and receptive-field structure in neurons of the anterior optic tract of the honeybee brain, PLoS One 19 (2024) e0310282, https://doi.org/10.1371/journal.pone.0310282.
[69] E. Neher, G.J. Augustine, Calcium gradients and buffers in bovine chromaffin cells, J. Physiol. 450 (1992) 273–301, https://doi.org/10.1113/jphysiol.1992.sp019127.
[70] J. Phillips, R. Muheim, M. Painter, J. Raines, C. Anderson, L. Landler, D. Dommer, A. Raines, M. Deutschlander, J. Whitehead, N.E. Fitzpatrick, P. Youmans, C. Borland, K. Sloan, K. McKenna, Why is it so difficult to study magnetic compass orientation in murine rodents? J. Comp. Physiol. A Neuroethol. Sens. Neural Behav. Physiol. 208 (2022) 197–212, https://doi.org/10.1007/s00359-021-01532-z.
[71] D.F. Reiff, J. Plett, M. Mank, O. Griesbeck, A. Borst, Visualizing retinotopic half-wave rectified input to the motion detection circuitry of Drosophila, Nat. Neurosci. 13 (2010) 973–978, https://doi.org/10.1038/nn.2595.